Journal of Sound and Vibration (2002) **255**(1), 129–146
doi:10.1006/jsvi.2001.4144, available online at http://www.idealibrary.com on IDEAL®

HIGH-WAVENUMBER ACOUSTIC RADIATION FROM A THIN-WALLED AXISYMMETRIC CYLINDER

G. M. Keith and N. Peake

Department of Applied Mathematics and Theoretical Physics, University of Cambridge, Silver Street, Cambridge CB3 9EU, England

(*Received* 30 *January* 2001, *and in final form* 31 *October* 2001)

The radiation from an axisymmetric thin-walled cylinder is determined by using the Geometrical Theory of Diffraction. The non-uniformities associated with this theory are corrected by using uniform asymptotic techniques, and the farfield velocity potential is calculated everywhere. The theory provides a paradigm for interpretation of geometrical features of the directivity pattern in the far field, and the results are discussed from this perspective. Comparison is made with analytical results obtained by using the Wiener–Hopf technique and the agreement is shown to be excellent. In particular, the uniform asymptotic techniques give the correct farfield form of the velocity potential in the principal lobe and predict the value at the peak of the principal lobe very accurately. This work provides a theoretical basis for the investigation of the radiation from asymmetric cylinder apertures, which has important applications in the noise reduction of aircraft, and which is discussed in a companion paper.

1. INTRODUCTION

In aircraft engines, such as those used on commercial airliners, considerable noise is generated by the fan. Though the generation of this noise is currently a subject of much theoretical interest, this paper focuses on its propagation and radiation into the far field, in particular the role of the engine nacelle in determining the farfield radiation pattern. Described in this paper is the radiation from an axisymmetric cylinder, which is used to model the radiation from a conventional, axisymmetric nacelle. A companion paper [1], contains a description of the application of the techniques developed here to asymmetric cylinders, which provide a model for novel nacelle configurations currently under consideration for future aeroengines [2]. The approach here is to develop realistic, high-frequency asymptotic approximations for the farfield velocity potential.

Ray theory, together with the Geometrical Theory of Diffraction (GTD) due to Keller [3, 4], provides a powerful analytical tool for establishing the leading order behaviour of non-trivial, high-frequency acoustic fields scattered by obstacles with non-trivial boundary geometries. Recently, Hocter [5], following Chapman [6], applied the GTD to the problem of the radiation from a thin-walled axisymmetric cylinder and, in the far field at certain observer locations, found excellent agreement with the exact solution, which can be calculated by using the Wiener–Hopf technique [7]. However, the field predicted by the GTD has certain non-uniformities corresponding to shadow and reflection boundaries and caustics, which require correction by using uniform asymptotic techniques. Without these corrections the GTD alone is unable to predict either the phase or the amplitude of the velocity potential near the center of the principal lobe, which is the region of highest radiated intensity. This failure of the GTD is a severe practical shortcoming.

0022-460X/02/$35.00

The uniform asymptotic techniques required to repair the GTD in these regions are the key to this paper. This paper begins with a brief recapitulation of the construction of the GTD field by using Chapman's ray description of propagating eigenmodes as input to a scattering problem, which is solved by using Keller's theory. The uniform asymptotic techniques are then described and the details of their implementation discussed. One of the great advantages of the GTD is the geometrical insight it provides into these radiation problems. The GTD is not only extremely effective at accurately predicting the radiated field, it also provides a useful paradigm for interpreting the geometrical features of this field. The results section begins with a discussion of a farfield directivity profile generated by the radiation of a typical duct eigenmode before attention is turned to a comparison between the results predicted by the GTD with its uniform asymptotic extensions and the exact solution. In a short conclusion, the efficacy and relevance of this theory compared with other approximate and exact techniques for calculating the sound field radiated from an axisymmetric cylinder will be briefly discussed.

2. DUCT RAYS AND THE GTD

This section opens with a presentation of Chapman's ray description of the field within the duct, and moves on to a description of the construction of the GTD field. Cylindrical polar co-ordinates x, ρ and ϕ and spherical polar co-ordinates R, θ and ϕ are used throughout (see Figure 1). Unsteady velocity potentials with harmonic time dependence $\exp(-i\omega t)$ are governed by the Helmholtz equation $\nabla^2 u + k^2 u = 0$, where $k = \omega/c$ and c is

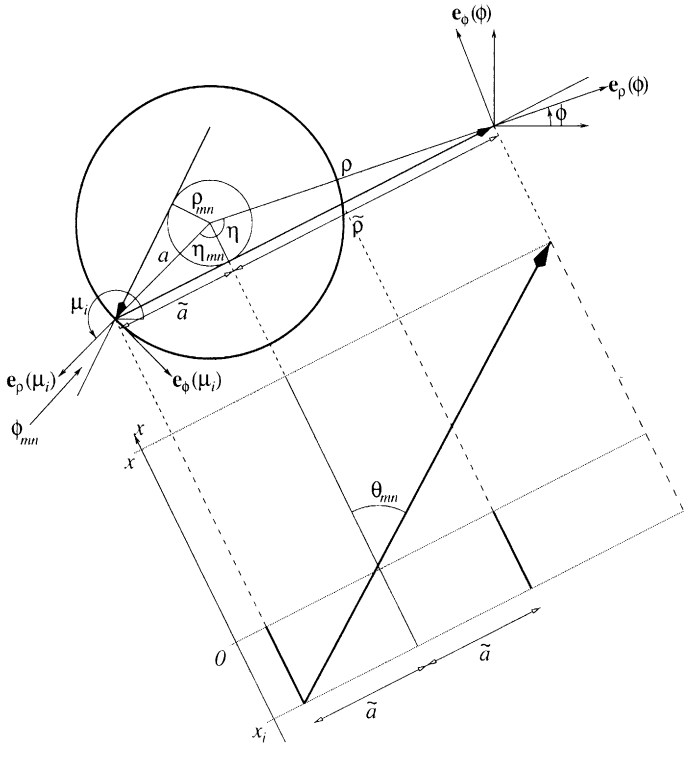

Figure 1. A ray reflected from the inside wall of the duct, in plan view of, respectively, the aperture and the plane on which the exiting ray propagates.

the speed of sound, which is assumed constant. The analysis is performed with no mean flow, but the inclusion of mean-flow effects may be easily achieved by using the Prandtl–Glauert transformation.

2.1. THE RAY FIELD IN THE DUCT

Eigensolutions to the velocity potential that satisfies the Helmholtz equation in a hard-walled cylindrical duct of circular cross-section with radius a, can be written

$$u_{mn} = \mathrm{e}^{\mathrm{i}(m\phi + k_x x)} \mathrm{J}_m(k_\rho \rho), \tag{1}$$

where m is the azimuthal mode number and J_m is the Bessel function of order m. The hard-wall boundary condition sets $k_\rho a = j'_{mn}$, where n is the radial mode number and j'_{mn} is the nth zero of J'_m. Only values of k_x that are real and positive, which correspond to cut-on modes propagating in the positive x direction, are considered here.

Following Chapman [6], define

$$\sin\theta_{mn} = \frac{j'_{mn}}{ka}, \qquad \sin\phi_{mn} = \frac{m}{j'_{mn}}, \qquad \rho_{mn} = a\sin\phi_{mn}, \tag{2}$$

where θ_{mn} and ϕ_{mn} are, respectively, the polar and azimuthal mode angles; ρ_{mn} is the caustic radius and the cylinder $\rho = \rho_{mn}$ is the caustic cylinder. Note that θ_{mn} is real provided $j'_{mn} < ka$, which is the condition that $k_\rho < k$ and $k_x = \sqrt{k^2 - k_\rho^2}$ is real. So θ_{mn} is real if the mode is cut-on. Chapman shows that for $\rho > \rho_{mn}$

$$u_{mn} \sim \sum_{+,-} \mathrm{e}^{\mathrm{i}\Psi^{\pm}} \left(\frac{1}{2\pi m} \frac{\rho_{mn}}{\rho} \right)^{1/2}, \tag{3}$$

where

$$\Psi^{\pm} = m\phi + xk\cos\theta_{mn} \pm (m\tan\eta - m\eta - \pi/4) \tag{4}$$

$$= k[a\sin\theta_{mn}\sin\phi_{mn}(\phi \mp \eta) + (x, \tilde{\rho})(\cos\theta_{mn}, \pm\sin\theta_{mn})] \mp \pi/4 \tag{5}$$

with

$$0 \leqslant \tilde{\rho} = \sqrt{\rho^2 - \rho_{mn}^2}, \quad \tan\eta = \tilde{\rho}/\rho_{mn}, \tag{6}$$

see Figure 2.

Examination of the amplitude in equation (3) and the form of the phase given by equation (5) reveals the ray structure of the propagating duct mode. The field at a point outside the caustic cylinder $\rho = \rho_{mn}$ is given, to leading order, by the sum of contributions from two rays passing through that point. These rays propagate on plane surfaces that are tangential to the caustic cylinder, at an angle θ_{mn} to a line parallel with the cylinder axis in these planes. One of the rays, corresponding to the " + " term in equations (3) and (5), is propagating outwards towards the duct wall and the other, corresponding to the " − " term in equations (3) and (5), is propagating inwards towards the caustic radius.

The rays obey the laws of geometrical acoustics at the duct walls. Here, the ray propagating inward from a point on the wall makes the same angle with the normal to the wall as the ray propagating outward toward the wall, and the two rays and the normal are coplanar. The difference in the phases of the two rays is, to the same order as equation (3),

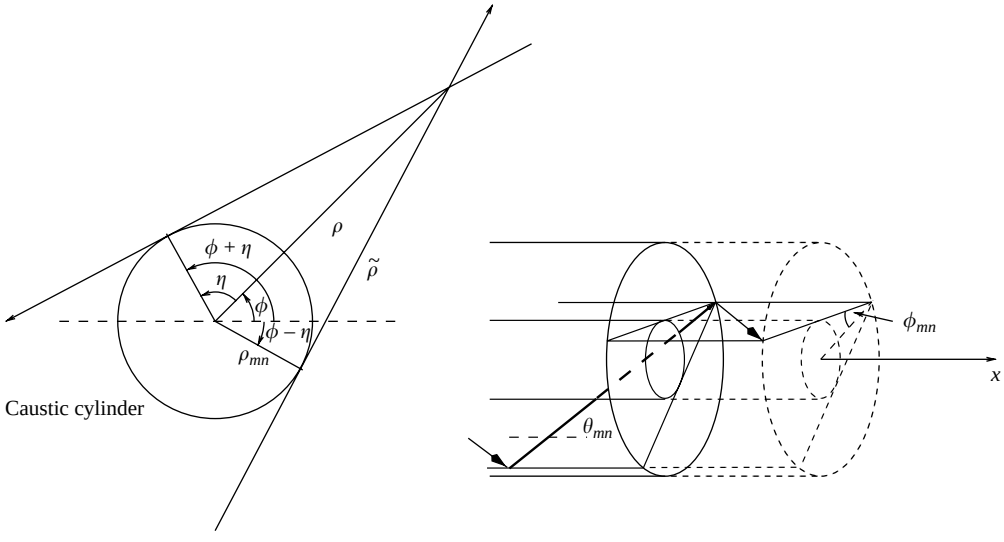

Figure 2. A plan view of two rays and the caustic cylinder, with ρ_{mn}, $\tilde{\rho}$ and η, and a ray propagating along the duct and forming part of a piecewise linear helix.

a multiple of 2π. In this fashion, a given ray propagates along the duct, reflecting several times from the duct wall to form a linear piecewise helix. As such a ray passes the caustic cylinder and its contribution switches from the " $-$ " term associated with inward propagating rays to the " $+$ " term associated with outward propagating rays, it undergoes a phase retardation of $\pi/2$ and its amplitude passes through a singularity. These features are typical of the behaviour of fields on rays near caustics and will be discussed in the context of a similar caustic that arises in the externally radiated field in section 2.3.

In the semi-infinite duct, Chapman's formulation may be used all the way up to where the rays begin to interact with the termination of the duct. The rays inside the duct are either reflected out of the duct or they strike the edge. The rays that are reflected out of the duct comprise the geometrical acoustics field and those that strike the edge instigate the diffracted rays that make up the diffracted field.

2.2. THE GEOMETRICAL ACOUSTICS FIELD

The field on the rays that comprise the geometrical acoustics field is calculated by using ordinary reflection theories of geometrical wave propagation. The leading-order term of the field on these rays is found to be

$$u_g(x, \rho, \phi) = A_g e^{ik s_g - i\pi/2} = e^{i(n-1)\pi} \left(\frac{1}{2\pi k \tilde{\rho} \sin \theta_{mn}} \right)^{1/2} e^{ik(s_i + \sigma_g) - i\pi/2} \tag{7}$$

with

$$s_i = \mu_i \rho_{mn} \sin \theta_{mn} + x_i \cos \theta_{mn} \tag{8}$$

given, after a little manipulation, by equation (4), and

$$x_i = x - (\tilde{\rho} + \tilde{a}) \cot \theta_{mn}, \tag{9}$$

$$\mu_i = \phi - \eta - \eta_{mn}, \qquad \sigma_g = (\tilde{\rho} + \tilde{a}) \csc \theta_{mn} \tag{10,11}$$

from Figure 1. The length $\tilde{a}$ and the angle η_{mn} are, respectively, the values of $\tilde{\rho}$ and η when $\rho = a$.

The rays of the geometrical acoustics field diverge cylindrically and, as such, would not satisfy the radiation condition in the far field. In fact, as shall soon be shown, the range of the validity of the geometrical acoustics field is very small as its rays quickly intrude into non-uniform regions. Nevertheless, the rays and the field on those rays must be calculated as they are required to determine the coefficients of the uniform expansions.

2.3. THE DIFFRACTED RAY FIELD

Keller's Geometrical Theory of Diffraction [3, 4] accounts for diffraction by the inclusion of a diffracted ray field constructed in the following way. Each point on the edge of the cylinder is a vertex to a cone of rays with semiangle, β, equal to the angle between the incident ray, whose direction is given by the unit vector $\mathbf{u}$, and the tangent to the edge, $\mathbf{t}$, at that point. Points insonified by the diffracted ray field are described by the diffracted ray transformation

$$\mathbf{x}(\mu, \nu, \sigma) = \boldsymbol{\gamma}(\mu) + \sigma \mathbf{v}(\mu, \nu), \tag{12}$$

where $\boldsymbol{\gamma}(\mu)$ describes the position on the edge and

$$\mathbf{v}(\mu, \nu) = (\cos \beta)\mathbf{t} + \sin \beta[(-\sin \nu)\mathbf{n} + (\cos \nu)\mathbf{b}], \tag{13}$$

where $\mathbf{n}$ and $\mathbf{b}$ are, respectively, the normal and binormal of the curve described by the edge. The ray co-ordinates μ, ν and σ, respectively, parameterize the edge, measure the angle round the cone of diffracted rays and measure the distance along diffracted rays from the point $\boldsymbol{\gamma}(\mu)$ to $\mathbf{x}$; see Figure 3.

In the case of the axisymmetric cylinder, μ is identical to the value of the azimuthal angle, ϕ, at the apex of the cone on the edge. The cone angle, β, is given by Keller's law of

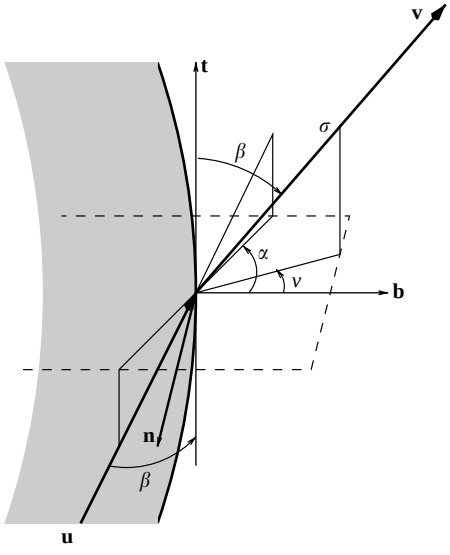

Figure 3. A ray, with direction $\mathbf{u}$, incident on the edge of the cylinder together with one of the diffracted rays, with direction $\mathbf{v}$, in the the cone of diffracted rays emanating from that point.

diffraction and

$$\cos\beta = \mathbf{u}\cdot\mathbf{t} = \sin\theta_{mn}\sin\phi_{mn} = m/ka. \tag{14}$$

The cone angle is constant around the edge and $\mathbf{v}$ is a function of μ only through the vectors $\mathbf{t}$ and $\mathbf{n}$. Following Chapman, the external geometry is expressed in terms, not of β, but of its complement the polar quiet angle $\theta_m = \pi/2 - \beta$. From equation (14),

$$\sin\theta_m = m/ka. \tag{15}$$

The leading-order term of the field on a diffracted ray is given through Keller's theory by

$$u_d = A_{inc}\mathrm{e}^{\mathrm{i}k(s_{inc}+\sigma)}D(v;\alpha)/|j|^{1/2}, \tag{16}$$

where A_{inc} and s_{inc} are, respectively, the amplitude and eikonal of the incident ray at the point of diffraction given by

$$A_{inc} = A_g(\rho = a), \qquad s_{inc} = s_g\ (x = 0,\ \rho = a). \tag{17,18}$$

If the diffracted ray has passed through the caustic surface, which is described below, the phase is retarded by $\pi/2$. The diffraction coefficient, D, is given by

$$D(v;\alpha) = \frac{\mathrm{e}^{\mathrm{i}\pi/4}}{2(2\pi k)^{1/2}}\left[\csc\left(\frac{v-\alpha}{2}\right) + \csc\left(\frac{v+\alpha}{2}\right)\right] \tag{19}$$

and is obtained through examination of the leading order asymptotics of the Sommerfield solution to the problem of the diffraction of a plane wave by a semi-infinite plate. The angle α is the value of the angle v on the continuation of the incident ray past the edge and is given by

$$\tan\alpha = \frac{\sin\theta_m}{\cos\theta_{mn}}. \tag{20}$$

The shadow and reflection boundaries are the surfaces $v = \pm\alpha$, respectively, and D contains non-integrable singularities at these points. These will be addressed in section 2.3.

The remaining quantity in equation (16) is j, the geometrical divergence of the ray transformation given by equation (12), taken with respect to arc length on the edge rather than the co-ordinate μ. It is given by

$$j = \sigma\cos^2\theta_m\left(1 + \frac{\sigma\sin v}{a\cos\theta_m}\right). \tag{21}$$

Clearly, $j = 0$ at certain points in the radiated field (caustic points) and u_d contains integrable singularities at these points. These too will be addressed in section 2.3.

It remains to find the ray co-ordinates, μ, v and σ, in terms of the co-ordinates of an observer location, R, θ and ϕ; i.e., to invert the ray transformation, equation (12). This can be done by algebraic manipulation of equation (12) and there are two physical solutions

$$\sigma^{\pm} = R\varsigma^{\pm}, \tag{22}$$

where

$$\varsigma^{\pm} = (\Gamma \pm 2\varepsilon\Delta^{1/2})^{1/2}, \tag{23}$$

with

$$\Gamma = 1 + \varepsilon^2(2\cos^2\theta_m - 1), \tag{24}$$

$$\Delta = \cos^2\theta_m - \cos^2\theta - \varepsilon^2\cos^2\theta_m \sin^2\theta_m \tag{25}$$

and $\varepsilon = a/R$. Equations for corresponding values of $\mu^{\pm}$ and $v^{\pm}$ follow, with

$$\sin v^{\pm} = \frac{-\varepsilon\cos^2\theta_m \mp \Delta^{1/2}}{\varsigma^{\pm}\cos\theta_m}, \tag{26}$$

$$\sin(\phi - \mu^{\pm}) = \frac{\varsigma^{\pm}\sin\theta_m}{\sin\theta}. \tag{27}$$

It follows from these calculations that there are exactly two or zero solutions to the ray-tracing problem accordingly as $\Delta > 0$ or < 0, respectively. Substituting equations (22) and (26) into equation (21) gives

$$j^{\pm} = \mp R\frac{\Delta^{1/2}\varsigma^{\pm}}{\varepsilon}, \tag{28}$$

so the caustic surface, $j = 0$, delineates two regions, one containing a two-component diffracted ray field and one into which no real diffracted rays penetrate. This region is called the quiet region, after Chapman. From equation (21), it may be seen $j > 0$ for σ close to zero. The value of j on the " + " ray in the far field is negative; it must pass through the caustic and change sign. In doing so its phase is retarded by $\pi/2$.

Away from shadow and reflection boundaries and the caustic, the diffracted field is given by summing the contribution from the diffracted rays that pass through a given point and

$$u_d = A_d^{+}\mathrm{e}^{\mathrm{i}ks_d^{+} - \mathrm{i}\pi/2} + A_d^{-}\mathrm{e}^{\mathrm{i}ks_d^{-}}, \tag{29}$$

where $A_d^{\pm}$ and $s_d^{\pm}$ are, respectively, the leading order amplitudes and phases of the two diffracted rays through a given point, given by equation (16).

3. UNIFORM ASYMPTOTICS

This section comprises a description of the uniform asymptotic expansions that smooth out the singularities in the GTD field, which were identified in the previous section.

3.1. THE CAUSTIC

An exact expression for the caustic surface is given by equation (25) with $\Delta = 0$. The caustic surface is the hyperboloid

$$\left(\frac{\cos\theta}{\cos\theta_m}\right)^2 - \left(\frac{\sin\theta}{\sin\theta_m}\right)^2 = \varepsilon^2, \tag{30}$$

which in the far field approaches the cone $\theta = \theta_m$.

On the caustic surface, where $j = 0$, contributions to the diffracted field given by the GTD have an integrable singularity, which can be dealt with using uniform asymptotic techniques

due to Ludwig [8]. An alternative expansion for the transition region close to the caustic is postulated. This expansion contains certain unknown functional coefficients, equations for which are determined by substituting the expansion into the Helmholtz equation and setting powers of k to zero. The expansion is such that solutions to these equations can be found so that when the leading-order terms of the trial expansion are evaluated asymptotically away from the caustic, the diffracted field given by the GTD is recovered.

The leading order terms of the caustic transition expansion, the caustic transition field, are

$$u_d = \mathrm{e}^{\mathrm{i}k\chi}[V(k^{2/3}\psi)g_0 - \mathrm{i}k^{-1/3}V'(k^{2/3}\psi)h_0] \tag{31}$$

with

$$\psi = \left[\tfrac{3}{4}(s_d^+ - s_d^-)\right]^{2/3}, \qquad \chi = \frac{s_d^+ - s_d^-}{2} \tag{32}$$

and

$$g_0 = \sqrt{\pi}k^{1/6}\mathrm{e}^{-\mathrm{i}\pi/4}(A_d^+ + A_d^-)\psi^{1/4}, \tag{33}$$

$$h_0 = \sqrt{\pi}k^{1/6}\mathrm{e}^{-\mathrm{i}\pi/4}(A_d^+ - A_d^-)\psi^{-1/4}. \tag{34}$$

Here

$$V(t) = \frac{1}{2\pi}\int_{-\infty}^{\infty} \mathrm{e}^{\mathrm{i}(t\tau - \tau^3/3)}\,\mathrm{d}\tau = \mathrm{Ai}(-t). \tag{35}$$

Away from the caustic, where ψ is $O(1)$ or larger and V and V' can be replaced by their large argument asymptotic forms,

$$V(t) \sim \frac{t^{-1/4}}{2\sqrt{\pi}} \sum_{+,-} \mathrm{e}^{\pm \mathrm{i}(2/3\,t^{3/2} - \pi/4)}, \tag{36}$$

$$V'(t) \sim \frac{\mathrm{i}t^{1/4}}{2\sqrt{\pi}} \sum_{+,-} \pm\, \mathrm{e}^{\pm \mathrm{i}(2/3\,t^{3/2} - \pi/4)}, \tag{37}$$

equation (31) becomes

$$u_d \sim A_d^+ \mathrm{e}^{\mathrm{i}ks_d^+ - \mathrm{i}\pi/2} + A_d^- \mathrm{e}^{\mathrm{i}ks_d^-}; \tag{38}$$

i.e., the diffracted field given by the GTD with the $\pi/2$ phase retardation on the " + " ray from where it has passed through the caustic.

Inside the caustic, $\mu^{\pm}$, $v^{\pm}$ and $\sigma^{\pm}$, given by equations (22)–(27), have complex values and take the form $\mu^{\pm} = \mu^r \pm \mathrm{i}\mu^i$, $v^{\pm} = v^r \pm \mathrm{i}v^i$ and $\sigma^{\pm} = R(\varsigma^r \pm \mathrm{i}\varsigma^i)$. The field inside the caustic is given by analytic continuation of ψ, χ, g_0 and h_0 through the caustic, using expressions for $A_d^{\pm}$ and $s_d^{\pm}$ with the complex values of the ray co-ordinates. Values for ς^r and ς^i follow directly from equation (23) and a little manipulation of the other ray-tracing equations gives

$$\sin[2(\phi - \mu^r)] = \frac{2\sin\theta_m}{\sin^2\theta}[\varsigma^r \varepsilon \sin^2\theta_m - \varsigma^i|\Delta|^{1/2}], \tag{39}$$

$$\sinh(2\mu^i) = \frac{2\sin\theta_m}{\sin^2\theta}[\varsigma^i \varepsilon \sin^2\theta_m + \varsigma^r|\Delta|^{1/2}]. \tag{40}$$

Then

$$\chi = R(\varepsilon\mu_r \sin\theta_m + \varsigma^r) \tag{41}$$

and

$$\psi = -(\tfrac{3}{2}\bar{\psi})^{3/2} \tag{42}$$

with

$$\bar{\psi} = -R(\varepsilon\mu_i \sin\theta_m + \varsigma^i). \tag{43}$$

It may be shown that $\bar{\psi}$ is always greater than zero away from the caustic and is zero on the caustic, so the argument of V and V' in equation (31) is real and negative inside the caustic. Both these functions decay exponentially with negative argument.

With $v^+ = \overline{v^-}$, $e^{-i\pi/4}D(v^+) = \overline{e^{-i\pi/4}D(v^-)}$, and

$$g_0 = \frac{2\sqrt{\pi}k^{1/6}a^{1/2}}{R|\Delta|^{1/4}}\Re\left[\frac{e^{-i\pi/4}D(v^+)}{(\varsigma^+)^{1/2}}\right]\left(\frac{3}{2}\bar{\psi}\right)^{1/6}, \tag{44}$$

$$h_0 = \frac{2\sqrt{\pi}k^{1/6}a^{1/2}}{R|\Delta|^{1/4}}\Im\left[\frac{e^{-i\pi/4}D(v^+)}{(\varsigma^+)^{1/2}}\right]\left(\frac{3}{2}\bar{\psi}\right)^{-1/6}, \tag{45}$$

which completes the field calculation inside the caustic. The field is not defined on the line $\theta = 0$; however, here $\bar{\psi} \to \infty$, and the exponential behaviour of V and V' dominate the algebraic singularities in the amplitude functions. The field on this line is taken to be zero.

3.2. THE SHADOW AND REFLECTION BOUNDARIES

Shadow and reflection transition fields are constructed in a similar way to the caustic transition field. An alternative shadow or reflection transition expansion is postulated for the transition region close to the relevant boundary, and equations for the functional coefficients of this expansion are determined by examining the alternative expansion under the Helmholtz operator and setting powers of k to zero. The functional coefficients are chosen to satisfy these equations and to give the GTD field when they are evaluated asymptotically away from the transition region. The form for the shadow and reflection transition expansion follows work by Ahluwalia *et al.* [9] and examination of the form of the full solution to the Sommerfield problem of the diffraction of a plane wave by a semi-infinite plate; for a complete description, see reference [10].

The shadow and reflection boundaries are the surfaces $v = \pm\alpha$ and occur when rays of the diffracted ray field are collinear with rays of the geometrical acoustics ray field. Each of the shadow and reflection transition expansions deals with a ray of the geometrical acoustics field and the one ray of the diffracted ray field collinear with it. The total field is taken to be the sum of the relevant transition field; i.e., the leading order term of the transition expansion, and the contribution from the remaining diffracted ray.

In the near field, the shadow and reflection transition regions are separated by a region insonified by the geometrical acoustics rays and this procedure is performed without difficulty. However, at a distance typically quite close to the aperture, the reflection and

shadow regions begin to overlap. In fact, it is the interaction of the two transition regions that corrects the cylindrical divergence of the geometrical acoustics field and spreads the associated sound power in such a way as to return a spherically divergent, though still highly directed, farfield velocity potential.

To proceed for the far field, the two non-uniform regions are still treated independently, i.e., a uniform asymptotic transition field is constructed that matches to the diffracted field on one side and would match to the geometrical acoustics field on the other. However, in the far field, because of the overlap of the two transition regions, the circumstances under which the geometrical acoustics field would be recovered from the transition field are never encountered. The geometrical acoustics field is written as the sum of two similar geometrical acoustics fields with half the amplitude, and transition expansions are constructed that deal with one of those half-fields and the ray of the diffracted field collinear with it. The total field is the sum of the two transition fields.

It is easily shown that the diffracted ray associated with the reflection transition region is the " + " ray and the ray associated with the shadow transition region is the " − " ray. Thus, the potential is

$$u = u^+ + u^-$$

with

$$u^+ = \mathrm{e}^{\mathrm{i}ks_g - \mathrm{i}\pi/2} A_g \mathscr{F}(k^{1/2}\xi_r) + \mathrm{e}^{\mathrm{i}ks_d^+ - \mathrm{i}\pi/2}\left[A_d^+ - \frac{\mathrm{e}^{\mathrm{i}\pi/4} A_g}{2\sqrt{\pi} k^{1/2}\xi_r} \right], \tag{46}$$

$$u^- = \mathrm{e}^{\mathrm{i}ks_g - \mathrm{i}\pi/2} A_g \mathscr{F}(k^{1/2}\xi_s) + \mathrm{e}^{\mathrm{i}ks_d^-}\left[A_d^- - \frac{\mathrm{e}^{\mathrm{i}\pi/4} A_g}{2\sqrt{\pi} k^{1/2}\xi_s} \right] \tag{47}$$

and

$$\mathscr{F}(z) = -\frac{\mathrm{e}^{\mathrm{i}\pi/4}}{\sqrt{\pi}} \int_0^z \mathrm{e}^{\mathrm{i}u^2} \mathrm{d}u \xrightarrow{z \to \pm\infty} \mp \frac{1}{2} + \frac{\mathrm{e}^{\mathrm{i}\pi/4} \mathrm{e}^{\mathrm{i}z^2}}{2\sqrt{\pi} z} \tag{48}$$

and

$$k\xi_r^2 = k(s_d^+ - s_g), \tag{49}$$

$$k\xi_s^2 = ks_d^- - \left[ks_g - \frac{\pi}{2} - 2(n-1)\pi \right], \tag{50}$$

with $k^{1/2}\xi_r$ negative for $-\pi/2 < v^+ < -\alpha$ and positive elsewhere and $k^{1/2}\xi_s$ negative for $-\pi/2 < v^- < \alpha$ and positive elsewhere. The form of equation (50) follows from the specification of s_g and details of the phase function in Chapman's formulation of the ray structure of the incident duct mode; see reference [10]. The parameters ξ_r and ξ_s are zero on, respectively, the reflection and shadow boundaries.

4. RESULTS

In both kinds of transition field, there are functions that, for large argument, are evaluated asymptotically to return the GTD field. How large the arguments of these functions must be before the error in taking the GTD over the transition field is acceptably small depends on the desired accuracy. The caustic transition field (31) is used when $k^{2/3}\psi < C$ and the shadow and reflection transition fields when $k^{1/2}\xi < D$. By looking at the next terms in the expansions of the functions V, V' and $\mathscr{F}$, it may be shown that the

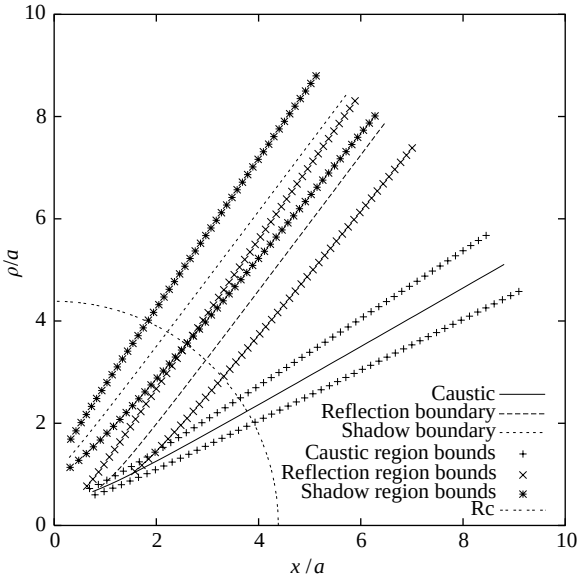

Figure 4. Exact location of the caustic, reflection and shadow boundaries and the boundaries of their corresponding transition regions for the mode $ka = 40$, $m = 20$, $n = 3$.

discrepancy between the transition field and the GTD is small ($< 4\%$) when, for the caustic and reflection/shadow transition fields, respectively, $C = 2{\cdot}4$ and $D = 3{\cdot}5$.

The exact locations of the various transition boundaries and their surrounding regions are shown in Figure 4 for the mode $ka = 40$, $m = 20$, $n = 3$. The boundaries are all hyperbolae and can be approximated for large R/a (small $\varepsilon = a/R$) by various cones. The caustic boundary is approximately $\theta = \theta_m$ and the reflection and shadow boundaries are approximately

$$\frac{\rho}{a} = \tan\theta_{mn}\left(\frac{x}{a} \mp \frac{\cos\phi_{mn}}{\tan\theta_{mn}}\right), \tag{51}$$

i.e., nested cones with semiangle θ_{mn}, the vertices of which are displaced from the aperture face by an amount $\pm\cos\phi_{mn}/\tan\theta_{mn}$ respectively; the shadow boundary is behind the reflection boundary.

To obtain approximate locations for the various transition regions, write $\theta = \theta_m + \Delta\theta_c$ close to the caustic and $\theta = \theta_{mn} + \Delta\theta_{r,s}$ close to the reflection and shadow boundaries, respectively, then expand $k^{2/3}\psi$ and $k^{1/2}\xi_{r,s}$ in powers of ε and these angular deviations to get

$$k^{2/3}\psi \sim (ka)^{2/3}\left(\frac{2\cos^3\theta_m}{\sin\theta_m}\right)^{1/3}\Delta\theta_c, \tag{52}$$

$$k^{1/2}\xi_{r,s} \sim \mp\left(\frac{kR}{2}\right)^{1/2}(\Delta\theta_{r,s} \pm \cos\theta_{mn}\cos\phi_{mn}), \tag{53}$$

whence the transition regions are found to be

$$\Delta\theta_c = \pm\frac{C}{(ka)^{2/3}}\left(\frac{\sin\theta_m}{2\cos^3\theta_m}\right)^{1/3} \tag{54}$$

for the caustic transition region and

$$\Delta\theta_r = -\cos\theta_{mn}\cos\phi_{mn}\frac{a}{R} \pm \frac{\sqrt{2}D}{(kR)^{1/2}}, \tag{55}$$

$$\Delta\theta_s = \cos\theta_{mn}\cos\phi_{mn}\frac{a}{R} \pm \frac{\sqrt{2}D}{(kR)^{1/2}} \tag{56}$$

for the reflection and shadow transition regions. Note, the reflection and shadow transition region boundaries cross at a distance R_c, where

$$\frac{R_c}{a} = \frac{ka}{2}\frac{\cos^2\theta_{mn}\cos^2\phi_{mn}}{C_2^2}; \tag{57}$$

see Figure 4.

For $R/a \gg R_c/a$, the second terms in the expressions (55) and (56) dominate and these transition regions are approximately the same. Within this angular sector, for $R/a \gg R_c/a$, it may be shown that the velocity potential has the correct farfield form to satisfy the radiation condition, i.e.,

$$u \sim \Omega(\theta, \phi; ka)\frac{e^{ikR}}{kR}. \tag{58}$$

This region is analogous to the Fraunhofer region that comes about, for example, in the diffraction of a plane wave through a slit. The distance corresponding to the Fresnel distance in that problem, which delineates the start of the Fraunhofer region and beyond which the directivity $|kRu|$ is a reasonable approximation to $\Omega = \lim_{R\to\infty}|kRu|$ is $\mathscr{R}$, where

$$\frac{\mathscr{R}}{a} = \frac{2}{\pi}ka\cos^2\theta_{mn}\cos^2\phi_{mn}. \tag{59}$$

This quantity is also related to the Rayleigh distance that is involved in the transition from nearfield to farfield behaviour in certain radiation problems. See reference [10] for a full description of the derivation of this quantity and more information regarding its significance.

From equation (59), in terms of the dimensionless radius R/a, the condition for farfield validity is

$$\frac{R}{a} > \frac{\mathscr{R}}{a} = (ka)\frac{2}{\pi}\cos^2\theta_{mn}\cos^2\phi_{mn}. \tag{60}$$

4.1. THE FARFIELD RADIATION PATTERN

Figure 5 shows a plot of $|kRu|$ against θ, a typical farfield directivity profile, with the locations of the various different GTD and transition regions. Here $C = 2{\cdot}4$ and $D = 3{\cdot}5$ and $R/a = 20 \gg \mathscr{R}/a \gg R_c/a$.

From $\theta = 0$ to the caustic there is the quiet region (1), into which no real rays penetrate and in which the field drops exponentially from its value at the caustic to zero. The caustic transition region (2) matches the value of the field at the caustic to the value predicted by the GTD in the first GTD region (3) between the caustic and the Fraunhofer region (4). The Fraunhofer region is discussed in the preceeding sections and is treated as the overlap

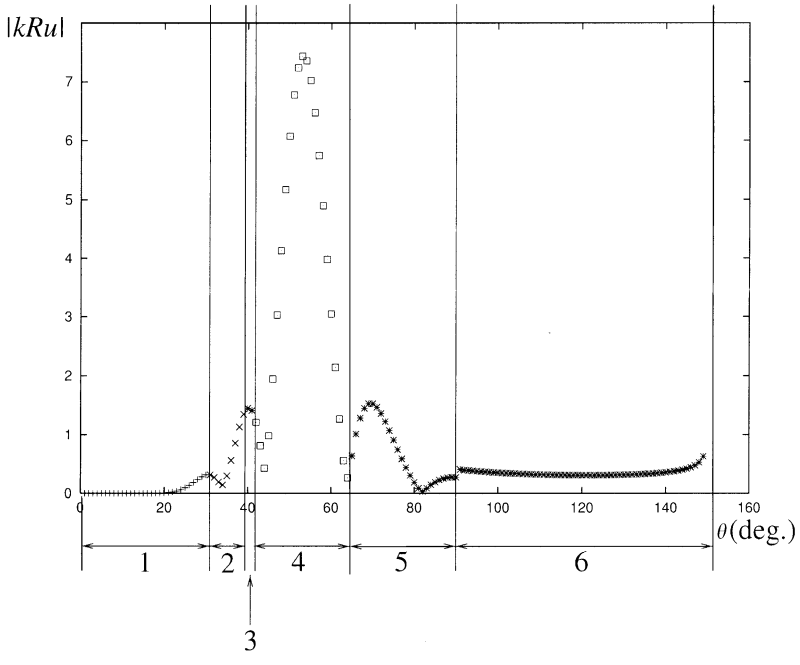

Figure 5. The directivity profile of the farfield radiation from an axisymmetric cylinder with a single incident mode ($ka = 40$, $m = 20$, $n = 3$) propagating in the duct.

between the reflection transition region and the shadow transition region. It smoothes over the non-integrable singularities in the diffracted field, accounts for the farfield manifestation of the high-energy region associated with the geometrical acoustics field in the near field and, crucially, provides a field value at the centre of the principal lobe. There follows a further GTD region (5) insonified by two diffracted rays up to the vertical plane where one of the rays is "switched off" as it is reflected into the duct. In the rearward arc there is another GTD region (6) with contributions from one diffracted ray up to the rearward caustic.

At the rearward caustic, there is a caustic type singularity in the diffracted field, but there is only one diffracted ray contribution, the other having been trapped by the duct. It is impossible to construct a caustic transition expansion as detailed above since that requires the full diffracted ray field—both contributions—and cannot deal with the artificial removal of one of them. One might be tempted to analytically continue the field on the single diffracted ray through the caustic, however by the time the GTD field—now carried by imaginary rays—is once more valid away from the caustic, its contribution is very close to zero.

4.2. COMPARISON WITH ANALYTIC RESULTS

In order to evaluate the accuracy of the GTD/UA field, the directivity plots given by our approach are compared with directivity plots given by the full analytical solution, which can be obtained by the Wiener–Hopf technique [7]. The full analytical results given below were generated by a code written by H.L. Meitz.

In Figure 6, directivity profiles are shown given by the GTD/UA field and the exact solution. The match is remarkable down to relatively low values of $ka \approx 8$ throughout

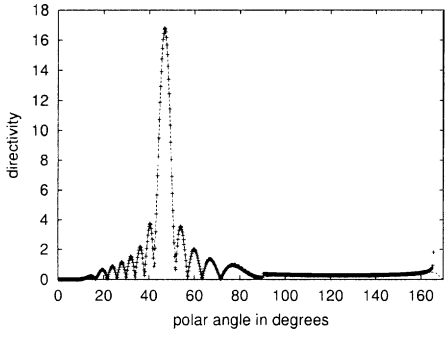

1. $ka = 60,\ m = 15,\ n = 8$

$\mathcal{R}/a = 15.8, R/a = 60$

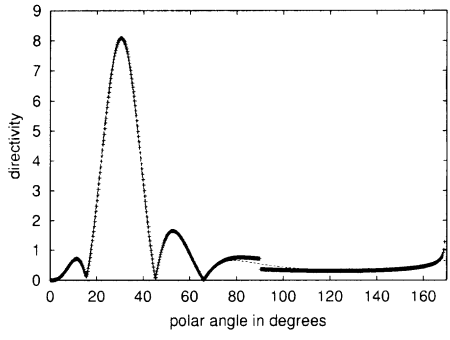

4. $ka = 16,\ m = 03,\ n = 2$

$\mathcal{R}/a = 6.54, R/a = 100$

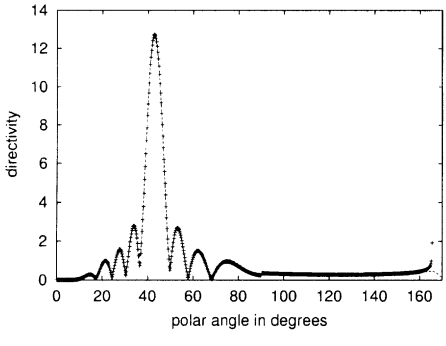

2. $ka = 40,\ m = 10,\ n = 5$

$\mathcal{R}/a = 11.8, R/a = 40$

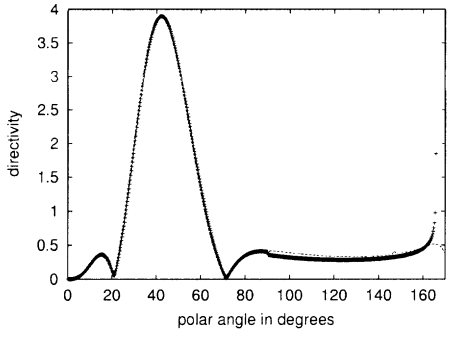

5. $ka = 12,\ m = 03,\ n = 2$

$\mathcal{R}/a = 3.60, R/a = 80$

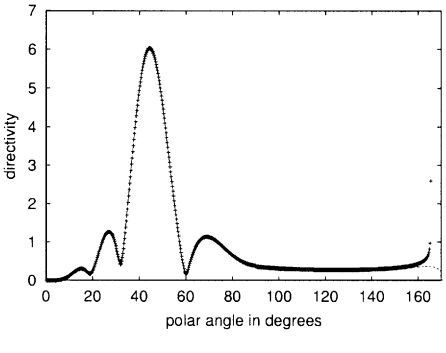

3. $ka = 20,\ m = 5,\ n = 3$

$\mathcal{R}/a = 5.65, R/a = 20$

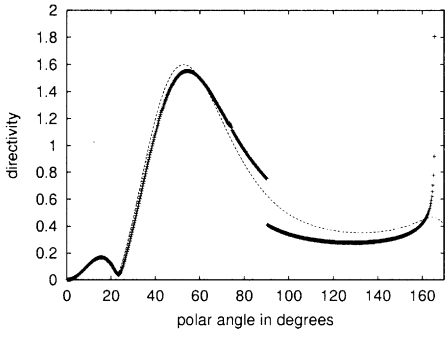

6. $ka = 8,\ m = 2,\ n = 2$

$\mathcal{R}/a = 1.32, R/a = 40$

Figure 6. Comparison of directivity profiles given by the GTD with uniform asymptotic extensions and full numerical calculation of the Wiener–Hopf integral, for different values of *ka*.

almost the entire far field: inside the quiet region, near the caustic, and of great importance, at the peak of the principal lobe where the geometrical acoustics transition regions overlap. The only noteworthy deviations are at the rearward caustic and, for low values of ka only, at the plane of the cylinder aperture.

The most cut-on modes may cause some difficulties with the uniform asymptotic theory, since here the caustic transition region and reflection transition region may overlap; likewise with the most cut-off modes when the reflection transition region transgresses the plane of the aperture. Both these difficulties can be avoided to some extent if there is no constraint as to how far into the farfield results may be given, as the angular extent of the reflection transition region diminishes with R/a. However, if the caustic transition region crosses the reflection boundary or if there is a constraint in our choice of observation radius, it may be possible to modify C and D to contain the transition region sufficiently to overcome these problems.

The mode closest to cut off may easily be accommodated by increasing the observation radius. The mode with $n = 2$ can be rendered by setting $R/a \approx 250$, however, in order to be able to compare it with analytical results, it is rendered for $R/a = 100$ with a fairly modest change to C and D. With $R/a = 100$ in the most cut-on mode, slightly more dramatic changes to C and D are required. However, reasonable comparisons are still possible with the present theory for this mode, although the results are no longer quite so impressively accurate at the peak of the principal lobe. Less absolute accuracy may be sacrificed at greater values of R/a and the asymptotic theory works adequately for R/a up to several hundreds of thousands, after which numerical errors start to undermine the code. However, doing so makes very little change to the directivity profile and in order to compare these results to analytical results, the observation radius must be maintained at more modest values.

Figure 7 shows directivity profiles for a range of radial modes with $ka = 50$ and $m = 12$, from the most cut-on mode $n = 1$ to the final propagating, almost cut-off mode $n = 11$. But for very small discrepancies near the caustic, the match is, once again, excellent, even for the most cut-on mode and the mode closest to cut off.

5. CONCLUSION

The application of uniform asymptotic techniques is essential to capture the behaviour of the externally radiated field in the most important regions near the principal lobe. The techniques described above accurately predict the amplitude and the phase of the radiated field over all but a small proportion of the far field for modes realistic in an aeroengine context.

Other uniform approximate theories have appeared in the literature. Notably Hocter [11] presents a uniform approximation based on the Weinstein U-function, which is also extremely accurate throughout most of the far field. In a manner curiously reminiscent of the theory presented above, the U-approximation also introduces a discontinuity in the farfield directivity at the plane of the aperture face. However, as in the present theory, the size of this deviation from the exact result diminishes with increasing values of ka. The U-approximation has the additional advantage of accurately predicting the farfield directivity across the rear caustic and in the rear quiet zone. Despite its accuracy and applicability, however, the U-approximation suffers from being derived from the exact solution acquired by using the Wiener–Hopf technique and, as such, cannot be extended to any other geometry. In particular, we believe that the U-approximation cannot be used to study the scarfed cylinder. The principal advantage of the U-approximation, therefore, is in

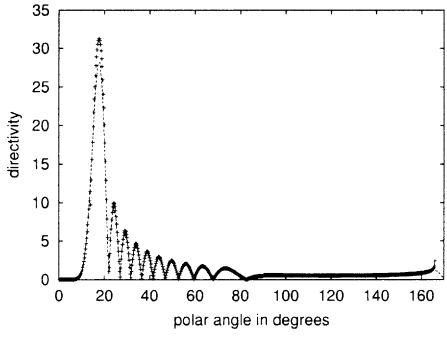

1. $ka = 50,\ m = 12,\ n = 1$

$\mathcal{R}/a = 8.16, R/a = 100$

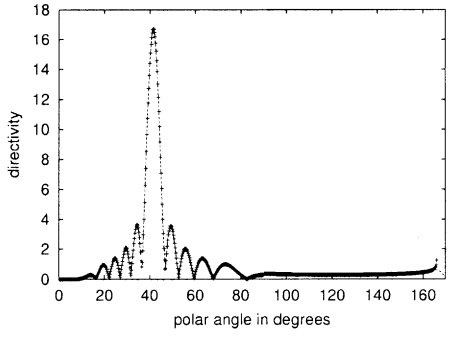

4. $ka = 50,\ m = 12,\ n = 6$

$\mathcal{R}/a = 15.5, R/a = 60$

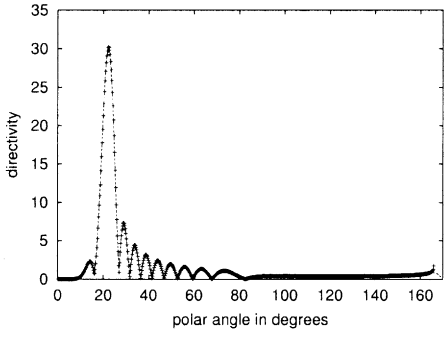

2. $ka = 50,\ m = 12,\ n = 2$

$\mathcal{R}/a = 16.2, R/a = 100$

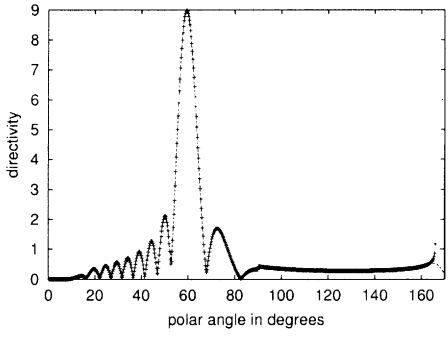

5. $ka = 50,\ m = 12,\ n = 9$

$\mathcal{R}/a = 7.36, R/a = 30$

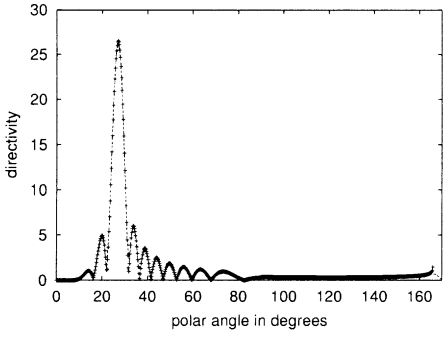

3. $ka = 50,\ m = 12,\ n = 3$

$\mathcal{R}/a = 18.2, R/a = 80$

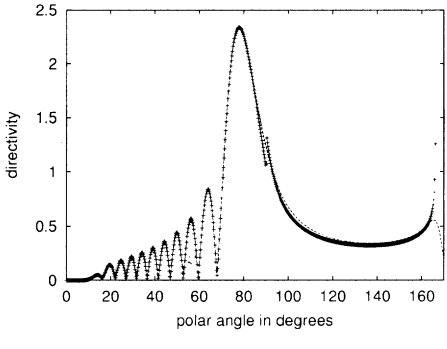

6. $ka = 50,\ m = 12,\ n = 11$

$\mathcal{R}/a = 0.49, R/a = 30$

Figure 7. Comparison of directivity profiles given by GTD with uniform asymptotic extensions and full numerical calculation of the Wiener–Hopf integral, for different radial orders. Here, $ka = 50$, $m = 12$ and there are 11 cut-on modes.

lightening the numerical burden of the exact Wiener–Hopf technique, and as computing power ever increases, this issue will become correspondingly less relevant.

Simpler approximations are also available. In particular, the Kirchhoff approximation is widely used, and is appealing on account of both the closed form of its solution and the simplicity of its underlying analysis. The closed form of solution offers dramatic gains in speed, and the expressions derived accurately predict the farfield directivity in a region close to the principal lobe. However, the result deviates from the exact solution close to the plane of the aperture face and can offer no information whatsoever about the directivity behind the plane of the aperture face. The underlying theory may be applied to more exotic geometries than the axisymmetric cylinder, but in doing so the solution loses its closed form and much of its simplicity. In such circumstances, we believe that the method's inaccuracy over much of the far field makes it, on the whole, a less attractive option that the methods set out in this paper.

The GTD coupled with the uniform asymptotic extensions described in this paper offer an attractive compromise between the accuracy and universal applicability of the Wiener–Hopf technique and the simplicity of the Kirchhoff method. As shown above, the method is remarkably accurate over the majority of the farfield and, as it too is in closed form (albeit a closed form rather more complicated than the results of the Kirchhoff analysis), it is extremely fast computationally. Despite the speed and surprising accuracy of our results, however, the major significance of the success of the GTD is in the relative ease with which it can be applied to more interesting boundary conditions. Specifically, there has been much interest recently in a novel aeroengine nacelle design, which incorporates a scarfed inlet whose aperture faces slightly upward away from the horizontal in an attempt to direct sound radiation away from the ground. The extension of these techniques, both the simple GTD and the uniform asymptotic theory, can be found in reference [10] and forms the subject of the companion paper [1].

ACKNOWLEDGMENTS

The authors would like to thank the EPSRC and Rolls Royce plc for their generous assistance to this research and Dr Hubert Meitz for his valuable advice and ongoing contribution.

REFERENCES

1. G. M. KEITH *Journal of Sound and Vibration*. The acoustic radiation from a thin-walled scarfed cylinder.
2. G. RAMAN and D. K. MCLAUGHLIN 1999 *Proceedings*: *AIAA Aeroacoustics*, *paper # AIAA*-99-1915. Highlights of the aeroacoustics research in the U.S.—1998.
3. J. B. KELLER 1958 *Calculus of Variations and its Applications*, *Proceedings of Symposia on Applied Mathematics* **8**, 27–52. A geometrical theory of diffraction.
4. J. B. KELLER 1962 *Journal of the Optical Society America* **52**, 116–130. Geometrical theory of diffraction.
5. S. T. HOCTER 2000 *Journal of Sound and Vibration* **231**, 1243–1256. Sound radiated from a cylindrical duct with Keller's geometrical theory.
6. C. J. CHAPMAN 1994 *Journal of Fluid Mechanics* **281**, 293–311. Sound radiation from a cylindrical duct. Part 1. Ray structure of the duct modes and of the external field.
7. L. A. WEINSTEIN 1969 *The Theory of Diffraction and the Factorisation Method*. Golem Press.
8. D. LUDWIG 1966 *Communications in Pure and Applied Mathematics* **19**, 215–250. Uniform asymptotic expansions at a caustic.

9. D. S. AHLUWALIA, R. M. LEWIS and J. BOERSMA 1968 *SIAM Journal of Applied Mathematics* **16**, 783–807. Uniform asymptotic theory of diffraction by a plane screen.
10. G. M. KEITH 2001 *Ph.D. Thesis*, *University of Cambridge*. A theoretical investigation into the radiation from an aeroengine.
11. S. T. HOCTER 1999 *Journal of Sound and Vibration* **227**, 397–407. Exact and approximate directivity patterns of the sound radiated from a cylindrical duct.